

Measurement of the Neutron Spin Structure Function g_1^n with a Polarized ^3He Internal Target

The HERMES Collaboration

K. Ackerstaff⁵, A. Airapetian³⁰, I. Akushevich⁶, N. Akopov³⁰, M. Amarian³⁰, E.C. Aschenauer^{12,22}, R. Avakian³⁰,
H. Avakian¹⁰, A. Avetissian³⁰, B. Bains¹⁴, S. Barrow²⁴, M. Beckmann¹¹, S. Belostotski²⁵, J.E. Belz^{4,28},
Th. Benisch⁸, S. Bernreuther⁸, N. Bianchi¹⁰, S. Blanchard²¹, J. Blouw²², H. Böttcher⁶, A. Borissov^{6,13}, J. Brack⁴,
B. Braun²⁰, B. Bray³, W. Brückner¹³, A. Brüll¹³, E.E.W. Bruins¹⁸, H.J. Bulten¹⁶, G.P. Capitani¹⁰, P. Carter³,
E. Cisbani²⁶, G.R. Court¹⁵, P.P.J. Delheij²⁸, E. Devitsin¹⁹, C.W. de Jager²², E. De Sanctis¹⁰, D. De Schepper¹⁸,
P.K.A. de Witt Huberts²², M. Düren⁸, A. Dvoredsky³, G. Elbakian³⁰, J. Emerson^{27,28}, A. Fantoni¹⁰,
A. Fechtchenko⁷, M. Ferstl⁸, D. Fick¹⁷, K. Fiedler⁸, B.W. Filippone³, H. Fischer¹¹, H.T. Fortune²⁴, J. Franz¹¹,
S. Frullani²⁶, M.-A. Funk⁵, N.D. Gagunashvili⁷, P. Galumian¹, H. Gao¹⁴, Y. Gärber⁶, F. Garibaldi²⁶, P. Geiger¹³,
V. Gharibyan³⁰, A. Golendoukhin^{17,30}, G. Graw²⁰, O. Grebenioug²⁵, P.W. Green^{1,28}, L.G. Greeniaus^{1,28},
C. Grosshauer⁸, A. Gute⁸, V. Gyurjyan¹⁰, J.P. Haas²¹, W. Haeberli¹⁶, J.-O. Hansen², D. Hasch⁶, O. Häusser^{27,28},
R.S. Henderson²⁸, Th. Henkes²², R. Hertenberger²⁰, Y. Holler⁵, R.J. Holt¹⁴, H. Ihssen⁵, M. Iodice²⁶, A. Izotov²⁵,
H.E. Jackson², A. Jgoun²⁵, C. Jones², R. Kaiser^{27,28}, E. Kinney⁴, M. Kirsch⁸, A. Kisselev²⁵, P. Kitching¹,
N. Koch¹⁷, K. Königsmann¹¹, M. Kolstein²², H. Kolster²⁰, W. Korsch³, V. Kozlov¹⁹, L.H. Kramer¹⁸, B. Krause⁶,
V.G. Krivokhijine⁷, M. Kückes^{27,28}, G. Kyle²¹, W. Lachnit⁸, W. Lorenzon²⁴, A. Lung³, N.C.R. Makins^{2,14},
S.I. Manaenkov²⁵, F.K. Martens¹, J.W. Martin¹⁸, A. Mateos¹⁸, K. McIlhany³, R.D. McKeown³, F. Meissner⁶,
D. Mercer⁴, A. Metz²⁰, N. Meyners⁵, O. Mikloukho²⁵, C.A. Miller^{1,28}, M.A. Miller¹⁴, R.G. Milner¹⁸, V. Mitsyn⁷,
A. Most¹⁴, R. Mozzetti¹⁰, V. Muccifora¹⁰, A. Nagaitsev⁷, Y. Naryshkin²⁵, A.M. Nathan¹⁴, F. Neunreither⁸,
M. Niczyporuk¹⁸, W.-D. Nowak⁶, M. Nupieri¹⁰, P. Oelwein¹³, H. Ogami²⁹, T.G. O'Neill², R. Openshaw²⁸,
V. Papavassiliou²¹, S.F. Pate^{18,21}, M. Pitt³, S. Potashov¹⁹, D.H. Potterveld², B. Povh¹³, G. Rakness⁴,
R. Redwine¹⁸, A.R. Reolon¹⁰, R. Ristinen⁴, K. Rith⁸, G. Röper⁵, H. Roloff⁶, P. Rossi¹⁰, S. Rudnitsky²⁴, M. Ruh¹¹,
D. Ryckbosch¹², Y. Sakemi²⁹, I. Savin⁷, K.P. Schüller⁵, A. Schwind⁶, T.-A. Shibata²⁹, T. Shin¹⁸, A. Simon^{11,21},
K. Sinram⁵, W.R. Smythe⁴, J. Sowinski¹³, M. Spengos²⁴, E. Steffens⁸, J. Stenger⁸, J. Stewart¹⁵, F. Stock¹³,
U. Stoesslein⁶, M. Sutter¹⁸, H. Tallini¹⁵, S. Taroian³⁰, A. Terkulov¹⁹, D.M. Thiessen^{27,28}, B. Tipton¹⁸,
A. Trudel^{27,28}, M. Tytgat¹², G.M. Urciuoli²⁶, R. Van de Vyver¹², J.F.J. van den Brand^{16,22}, G. van der
Steenhoven²², M.C. Vetterli^{27,28}, E. Volk¹³, W. Wander⁸, T.P. Welch²³, S.E. Williamson¹⁴, T. Wise¹⁶, T. Wölfel⁸,
K. Zapfe-Düren⁵, H. Zohrabian³⁰, R. Zurmühle²⁴

¹University of Alberta, Edmonton, Alberta T6G 2N2, Canada

²Argonne National Laboratory, Argonne, Illinois 60439, USA

³W.K.Kellogg Radiation Lab, California Institute of Technology, Pasadena, CA, 91125, USA

⁴University of Colorado, Boulder CO 80309-0446, USA

⁵DESY, Deutsches Elektronen Synchrotron, 22603 Hamburg, Germany

⁶DESY-IfH Zeuthen, 15738 Zeuthen, Germany

⁷Joint Institute for Nuclear Research, 141980 Dubna, Russia

⁸Physikalisches Institut der Universität Erlangen-Nürnberg, 91058 Erlangen, Germany

¹⁰Istituto Nazionale di Fisica Nucleare, Laboratori Nazionali di Frascati, 00044 Frascati, Italy

¹¹Fakultät für Physik, Universität Freiburg, 79104 Freiburg, Germany

¹²University of Gent, 9000 Gent, Belgium

¹³Max-Planck-Institut für Kernphysik, 69029 Heidelberg, Germany

¹⁴University of Illinois, Urbana, Illinois 61801, USA

¹⁵University of Liverpool, Liverpool L693BX, United Kingdom

¹⁶University of Wisconsin-Madison, Madison, Wisconsin 53706, USA

¹⁷Philipps-Universität Marburg, 35037 Marburg, Germany

¹⁸Laboratory for Nuclear Science, Massachusetts Institute of Technology, Cambridge, MA 02139, USA

¹⁹Lebedev Physical Institute, 117924 Moscow, Russia

²⁰Sektion Physik der Universität München, 85748 Garching, Germany

²¹New Mexico State University, Las Cruces, NM 88003, USA

²²Nationaal Instituut voor Kernfysica en Hoge-Energiefysica (NIKHEF), 1009 DB Amsterdam, The Netherlands

²³Oregon State University, Corvallis, Oregon 97331, USA

²⁴University of Pennsylvania, Philadelphia PA 19104-6396, USA

²⁵Petersburg Nuclear Physics Institute, St.Petersburg, 188350 Russia

²⁶Istituto Superiore di Sanita, Physics Laboratory and Istituto Nazionale di Fisica Nucleare, Sezione Sanita, 00161 Rome, Italy

²⁷Simon Fraser University, Burnaby, British Columbia V5A 1S6 Canada

²⁸TRIUMF, Vancouver, British Columbia V6T 2A3, Canada

Results are reported from the HERMES experiment at HERA on a measurement of the neutron spin structure function $g_1^n(x, Q^2)$ in deep inelastic scattering using 27.5 GeV longitudinally polarized positrons incident on a polarized ^3He internal gas target. The data cover the kinematic range $0.023 < x < 0.6$ and $1 (\text{GeV}/c)^2 < Q^2 < 15 (\text{GeV}/c)^2$. The integral $\int_{0.023}^{0.6} g_1^n(x) dx$ evaluated at a fixed Q^2 of $2.5 (\text{GeV}/c)^2$ is $-0.034 \pm 0.013(\text{stat.}) \pm 0.005(\text{syst.})$. Assuming Regge behavior at low x , the first moment $\Gamma_1^n = \int_0^1 g_1^n(x) dx$ is $-0.037 \pm 0.013(\text{stat.}) \pm 0.005(\text{syst.}) \pm 0.006(\text{extrapol.})$.

PACS numbers: 25.30.Fj, 13.88.+e, 13.60.Hb

Deep inelastic scattering with lepton beams is an important tool for understanding the quark-gluon structure of the nucleon. With polarized beams and targets, the spin structure of the nucleon is probed via scattering of charged leptons from nucleons through the exchange of virtual photons (with energy transfer ν and squared four momentum $-Q^2$). Inclusive polarized scattering is characterized by two structure functions: $g_1(x, Q^2)$ and $g_2(x, Q^2)$, with $x = Q^2/2M\nu$. The structure function g_1 is determined from the virtual photon asymmetries A_1 and A_2 via

$$g_1 = \frac{F_1}{(1 + \gamma^2)} [A_1 + \gamma A_2], \quad (1)$$

where F_1 is the unpolarized structure function and $\gamma^2 = Q^2/\nu^2$.

In the quark parton model the structure function g_1 is related to the quark spin distributions Δq_f through

$$g_1(x, Q^2) = \frac{1}{2} \sum_f e_f^2 \Delta q_f(x, Q^2), \quad (2)$$

where the sum is over quark flavors; e_f is the quark charge in units of the elementary charge e , and x is interpreted as the fraction of the nucleon's light cone momentum carried by the struck quark. Important information can be obtained from the structure function integrals for proton and neutron $\Gamma_1^p = \int_0^1 g_1^p(x) dx$ and $\Gamma_1^n = \int_0^1 g_1^n(x) dx$. The fundamental Bjorken sum rule relates the difference $\Gamma_1^p - \Gamma_1^n$ to the weak axial charge g_A [1]. Including QCD corrections [2,3], this sum rule has been confirmed experimentally within about 10 percent, while the model dependent Ellis-Jaffe sum rules [4], which provide predictions for Γ_1^p and Γ_1^n separately, are significantly violated [5–15]. The experimental results suggest that only a fraction of the nucleon's spin is due to the quark spins, and that the remainder results from gluons or orbital angular momentum.

HERMES is based on two novel techniques: an internal gas target of polarized atomic hydrogen, deuterium or ^3He , and a high current longitudinally polarized positron beam circulating in a high-energy storage ring. A measurement of g_1^n extracted from data taken during the initial running of the HERMES experiment is reported in

this letter. The experiment utilized a 27.5 GeV beam of longitudinally polarized positrons in the HERA storage ring at DESY incident on a longitudinally polarized ^3He internal target [16–18].

The positron beam in the HERA ring becomes transversely polarized to a high level by the Sokolov-Ternov mechanism [19]. The time constant for this process depends on the beam energy and the beam tune and is approximately 20-25 minutes. Precise alignment of the machine quadrupoles and fine tuning of the orbit parameters are needed to achieve high polarisation. The required longitudinal polarization direction is obtained using spin rotators located upstream and downstream of the HERMES experiment in the East straight section of HERA. This results in the first longitudinally polarized electron beam in a high-energy storage ring [20]. The transverse polarization was measured continuously using Compton backscattering of circularly polarized laser light. Values of the equilibrium polarization in the range 40% to 65% were obtained under normal running conditions. Experimental data were analyzed only when the polarization was above 40% to reduce sensitivity to systematic effects. The average polarization for the analyzed data was 55%. The fractional statistical error for a single 60 s polarization measurement was typically 1-2% and the overall fractional systematic error was 5.4%, dominated by the uncertainty in the calibration of the beam polarimeter. A single beam polarization direction was used for the present measurements.

The ^3He target atoms were polarized by spin exchange collisions with ^3S metastable ^3He atoms in a glass cell. The ^3S atoms were produced by a weak RF discharge and polarized by optical pumping with 1083 nm laser light [21]. The polarized atoms diffused from the glass pumping cell into a 400 mm long open ended thin-walled storage cell inside the positron ring [22]. The storage cell was constructed of 125 μm thick ultrapure aluminum and was cooled to typically 25 K [23]. This provided a target of pure atomic species with an areal density of approximately 3.3×10^{14} atoms/cm². The polarization direction was defined by a 3.5 mT magnetic field parallel to the beam direction.

The polarization of the ^3He gas in both the pumping and the storage cells was measured continuously with op-

tical polarimeters [24]. The nuclear polarization in the pumping cell was determined from the polarization of emitted photons produced via atomic excitation by the RF discharge. A second polarimeter monitored the polarization in the storage cell by measuring the polarization of photons emitted from atoms that were excited by the positron beam. These measurements were used to investigate the possibility that atoms were depolarized in the storage cell. No evidence for such effects was found. Cell wall depolarization was measured at lower temperatures using this technique in dedicated test measurements [25]. The average value of the target polarization during the experiment was 46% with a fractional uncertainty of 5%. The target polarisation direction was reversed every 10 min by reversing the laser helicity.

The luminosity was measured by detecting Bhabha scattered target electrons in coincidence with the scattered positrons in a pair of NaBi(WO₄)₂ electromagnetic calorimeters. During the course of one positron fill (typically 8 hr), the positron current in the ring decreased from typically 30 mA at injection to ~ 10 mA, at which point the positron beam was dumped.

A schematic diagram of the apparatus [18] is shown in Fig. 1. It consists of a large dipole magnet surrounding the positron and proton beam pipes of HERA. The beam is shielded from the spectrometer's magnetic field by a horizontal iron plate. The spectrometer is constructed as two identical halves, mounted above and below the region of the beam pipes and the horizontal iron plate. The scattering angle acceptance of the spectrometer is $40 \text{ mrad} < \theta < 220 \text{ mrad}$. Each half contains thirty-six drift chamber planes for tracking. A pattern-matching algorithm and momentum look-up method [26] provides fast track reconstruction. A momentum resolution of 1 - 2% for positrons, depending on kinematics, and an average angular resolution of 0.6 mrad was achieved. The trigger was formed from a coincidence between a pair of scintillator hodoscope planes and a Pb-glass calorimeter. The trigger required an energy of greater than 3.5 GeV deposited in the calorimeter, resulting in a typical event rate of 50 Hz. Positron identification was accomplished using the calorimeter, the second hodoscope, which was preceded by 2 radiation lengths of Pb and functioned as a preshower counter, six transition radiation detector modules, and a N₂ threshold gas Cerenkov counter. This system provided positron identification with an average of 98% efficiency and a hadron contamination $< 1\%$. A two-stage collimator system mounted upstream of the target cell provided shielding from the synchrotron radiation generated in the beam bending and focussing components and from beam-halo positrons. With proper beam tuning, the detector system was essentially free of electromagnetic background from such processes. A negligible number of triggers from particles scattering from the storage cell walls were observed.

The structure function g_1^n was extracted from the

measured longitudinal asymmetry $A_{||}$ of the scattering cross section using Eq. (1) with $A_1 = A_{||}/D - \eta A_2$ and $F_1 = F_2(1 + \gamma^2)/(2x(1 + R))$. Here $D = [1 - (1 - y)\epsilon]/(1 + \epsilon R)$ is the virtual photon depolarization factor, $\epsilon = [4(1 - y) - \gamma^2 y^2]/[2y^2 + 4(1 - y) + \gamma^2 y^2]$ is the degree of transverse polarization of the virtual photon, $\eta = \epsilon\gamma y/[1 - \epsilon(1 - y)]$, $R = \sigma_L/\sigma_T$ is the longitudinal-to-transverse virtual photon cross-section ratio, $y = \nu/E$ and E is the beam energy. The magnitude of A_2 is constrained to be less than \sqrt{R} and has been measured previously [7] to be consistent with zero within large errors. Thus its contribution to g_1 was neglected but its uncertainty was included as a systematic error.

The value of $A_{||}/D$ for ³He was extracted from the measured counting rates using the formula

$$\frac{A_{||}}{D} = \frac{N^-L^+ - N^+L^-}{D(N^-L_P^+ + N^+L_P^-)}, \quad (3)$$

where $N^+(N^-)$ is the counting rate for target spin parallel (anti-parallel) to the beam spin, L^\pm are the deadtime-corrected luminosities for each target spin state, and L_P^\pm are the deadtime-corrected luminosities weighted by the product of the magnitudes of the beam and target polarizations for each spin state. This quantity was binned in x and y to take into account the strong variation of D with y and was determined separately for each positron fill.

After applying data quality criteria and kinematic cuts ($Q^2 > 1 \text{ (GeV/c)}^2$, $W^2 > 4 \text{ (GeV/c)}^2$ and $y < 0.85$) 2.7×10^6 events were available for the asymmetry analysis. Corrections were applied to account for background from charge symmetric processes (eg. $\gamma \rightarrow e^+e^-$), and from misidentified hadrons. Whereas the asymmetry of the former source was consistent with zero, the latter exhibited a non-zero asymmetry which was typically 20-50% of the positron asymmetry. The corrections from both backgrounds were at most 2% of the asymmetry for the smallest x bins and were negligible for large x values. QED radiative corrections were applied using the standard procedure [28], with corrections of typically 20% of the observed asymmetry. Monte Carlo simulations showed that smearing corrections due to the finite resolution of the spectrometer are negligible.

Corrections for nuclear effects are required to determine the neutron structure function g_1^n with a ³He target. The wave function for ³He is dominated by the configuration with the protons paired to zero spin. Therefore, most of the asymmetry from ³He is due to the neutron [29]. A detailed calculation [30] shows that binding effects and Fermi motion are negligible in extracting g_1^n from polarized ³He data, and that nuclear effects can be largely treated as a dilution due to scattering from the two largely unpolarized protons. A correction for the non-zero polarization of the protons (-0.028 ± 0.004), using the E-143 results for A_1^p [13], and the neutron polarization (0.86 ± 0.02) [30] has been included.

The extracted virtual photon asymmetry $A_1^n(x)$ is presented in Fig. 2(a). The averaged kinematic quantities and asymmetry results are listed in Table I. The corresponding $g_1^n(x)$, extracted from equation (1) and using parameterizations of the unpolarized structure function F_2 [31] and R [32], is shown in Fig. 2(b) and compared with the previous ^3He experiment from SLAC E-142 [7]. The systematic uncertainties in the present experiment are small compared to the statistical uncertainties, as indicated by the error bands in Fig. 2. The statistical uncertainties have been extracted from the observed fluctuations of the positron yields and exceed the uncertainty calculated from the number of events by 10%. The dominant sources of systematic errors on $A_{||}/D$ are the uncertainties in the measured beam and target polarization. In addition for g_1^n there are contributions of similar size which result from uncertainties in radiative corrections and nuclear corrections, and smaller contributions from the uncertainties in the knowledge of F_2^n , A_2 and R .

For an evaluation of the Ellis-Jaffe sum rule the integral of $g_1^n(x)$ must be determined at a fixed Q^2 and an extrapolation into the unmeasured x regions must be made. This requires an assumption on the Q^2 dependence of either A_1 or g_1 . To evolve g_1 to a fixed value of $Q_0^2 = 2.5 \text{ (GeV}/c)^2$, which is near to the mean Q^2 value of the data ($2.3 \text{ (GeV}/c)^2$), the assumption that A_1 is independent of Q^2 over the limited Q^2 range of our data has been used. This assumption is consistent with existing data [27]. Next-to-Leading-Order (NLO) QCD evolution [3,33] gives a slightly different result that changes the integral of g_1^n over the measured x range by $< 5\%$. Including this difference in the systematic error yields $\int_{0.023}^{0.6} g_1^n(x, Q_0^2) dx = -0.034 \pm 0.013(\text{stat.}) \pm 0.005(\text{syst.})$.

For the large x extrapolation, we used a parameterization for F_2^n [31] and assumed several models for the behavior of A_1^n for $x > 0.6$. Since A_1^n is expected [34] to approach unity for $x \rightarrow 1$, we considered a linear increase for A_1^n from 0 at $x = 0.6$ to 1 at $x = 1$ as well as the parameterization of ref. [35]. These studies indicate that $\int_{0.6}^1 g_1^n(x) dx = 0.002 \pm 0.003$. For the low x extrapolation there is no clear prediction. For comparison with previous measurements [7–9,11,12], we quote the integral Γ_1^n assuming a simple Regge parameterization at low x [36,37] of $g_1 \propto x^{-\alpha}$ with α in the range $-0.5 - 0$ fitted to the data for $x < 0.1$. This gives $\int_0^{0.023} g_1^n(x) dx = -0.005 \pm 0.005$, where a 100% uncertainty has been assigned to the value. However, it should be noted that recent work [3] indicates that a NLO treatment of the low x region could yield different results for the low x extrapolation. Combining the contributions from different x regions leads to a total integral of $\int_0^1 g_1^n(x, Q_0^2) dx = -0.037 \pm 0.013(\text{stat.}) \pm 0.005(\text{sys.}) \pm 0.006(\text{extrapol.})$ in good agreement with the value from experiment E-142 [7] using ^3He and the SMC [14,15] and E-143 [13,10] experiments using the difference of deuteron and proton.

In summary, the neutron spin structure function g_1^n has been measured with a polarized ^3He target. The results are in agreement with those of the SLAC E-142 experiment, but have been determined with an entirely new technique – a windowless polarized internal target with pure atomic species in a positron storage ring. Semi-inclusive asymmetries extracted from the present data set will be presented in a future publication.

We gratefully acknowledge the DESY management for its support and the DESY staff and the staffs of the collaborating institutions for their significant effort. This work was supported by the U. S. Department of Energy and National Science Foundation; the Natural Sciences and Engineering Research Council of Canada; the German Bundesministerium für Bildung, Wissenschaft Forschung und Technologie, the German Academic Exchange Service (DAAD); the Italian Istituto Nazionale di Fisica Nucleare; Monbusho International Scientific Research Program, JSPJ, and Toray Science Foundation of Japan; the Dutch Foundation for Fundamental Research of Matter; the NFWO/IKW, Belgium and the INTAS contribution from the European Community,

-
- [1] J.D. Bjorken, Phys. Rev.148 (1966) 1467; J.D. Bjorken, Phys. Rev. D 1 (1970) 1376.
 - [2] S.A. Larin, Phys. Lett. B334 (1994) 192.
 - [3] R. D. Ball, S. Forte and G. Ridolfi, Phys. Lett. B378 (1996) 255.
 - [4] J. Ellis and R.L. Jaffe, Phys. Rev. D 9 (1974) 1444; Phys. Rev. D 10 (1974) 1669.
 - [5] J. Ashman *et al.*, Phys. Lett. B206 (1988) 364.
 - [6] P.L. Anthony *et al.*, Phys. Rev. Lett. 71 (1993) 959.
 - [7] P.L. Anthony *et al.*, Phys. Rev. D 54 (1996) 6620.
 - [8] B. Adeva *et al.*, Phys. Lett. B302 (1993) 533.
 - [9] D. Adams *et al.*, Phys. Lett. B357 (1995) 248.
 - [10] K. Abe *et al.*, Phys. Rev. Lett. 75 (1995) 25.
 - [11] D. Adams *et al.*, Phys. Lett. B329 (1994) 399.
 - [12] B. Adeva *et al.*, Phys. Lett. B320 (1994) 400.
 - [13] K. Abe *et al.*, Phys. Rev. Lett. 74 (1995) 346.
 - [14] D.Adams *et al.*,preprint CERN-PPE/97-08
 - [15] D.Adams *et al.*, preprint hep-ex/9702005.
 - [16] HERMES Collaboration, K. Coulter *et al.*, *Proposal*, DESY-PRC 90/01 (1990); *Technical Design Report*, DESY-PRC 93/06 (1993).
 - [17] M. Düren, *The HERMES Experiment: From the Design to the First Results*, Habilitation thesis, Univ. Erlangen-Nürnberg; DESY-HERMES 95-02 (1995).
 - [18] HERMES Collaboration, *The HERMES spectrometer*, DESY-HERMES 97/9, (1997), to be published.
 - [19] A.A. Sokolov and I.M. Ternov, Sov. Phys. Doklady 8 (1964) 1203.
 - [20] D.P. Barber *et al.*, Phys. Lett. B343 (1995) 436.
 - [21] F. D. Colegrove, *et al.*, Phys. Rev. **132**, 2561 (1963); T.

- R. Gentile and R. D. McKeown, Phys. Rev. **A47** 456 (1993).
- [22] K. Lee, *et al.*, Nucl. Instr. Meth. **A 333**, (1993) 294; S. F. Pate *et al.*, Int. Workshop on Polarized Beams and Polarized Gas Targets, ed. Hans Paetz gen. Schieck and Lutz Sydow (World Scientific, London 1996) pp. 39-43.
- [23] L. H. Kramer, *et al.*, Nucl. Instr. Meth. **A365** 49 (1995).
- [24] W. Lorenzon, *et al.*, Phys. Rev. **A47** 468 (1993); M. L. Pitt *et al.*, Int. Workshop on Polarized Beams and Polarized Gas Targets, ed. Hans Paetz gen. Schieck and Lutz Sydow (World Scientific, London 1996) pp. 400-407.
- [25] W. Korsch, *et al.* Nucl. Instr. Meth. (in press).
- [26] W. Wander, *Rekonstruktion hochenergetischer Streuergebnisse im HERMES Experiment*, Ph.D. thesis, Univ. Erlangen-Nürnberg (1996).
- [27] K. Abe *et al.*, Phys. Lett. B364 (1995) 61.
- [28] I.V. Akushevich and N.M. Shumeiko, J. Phys. G: Nucl. Part. Phys. 20 (1994) 513.
- [29] J.L. Friar *et al.*, Phys. Rev. C 42 (1990) 2310.
- [30] C. Ciofi degli Atti *et al.*, Phys. Rev. C 48 (1993) R968.
- [31] NMC, M. Arneodo *et al.*, Phys. Lett. B364 (1995) 107, P. Amaudruz *et al.*, Phys. Lett. B295 (1992) 159.
- [32] L.W. Whitlow *et al.*, Phys. Lett. B250 (1990) 193.
- [33] M. Gluck, E. Reya and M. Stratmann, Phys. Rev. D53, (1996) 4775.
- [34] G. R. Farrar and D. R. Jackson, Phys. Rev. Lett. 35 (1975) 1416, G. R. Farrar, Phys. Lett. B70 (1977) 346.
- [35] A. Schaefer, Phys. Lett. B208 (1988) 175.
- [36] R. Heimann, Nucl. Phys. B64 (1973) 429.
- [37] J. Ellis and M. Karliner, Phys. Lett. B213 (1988) 73.

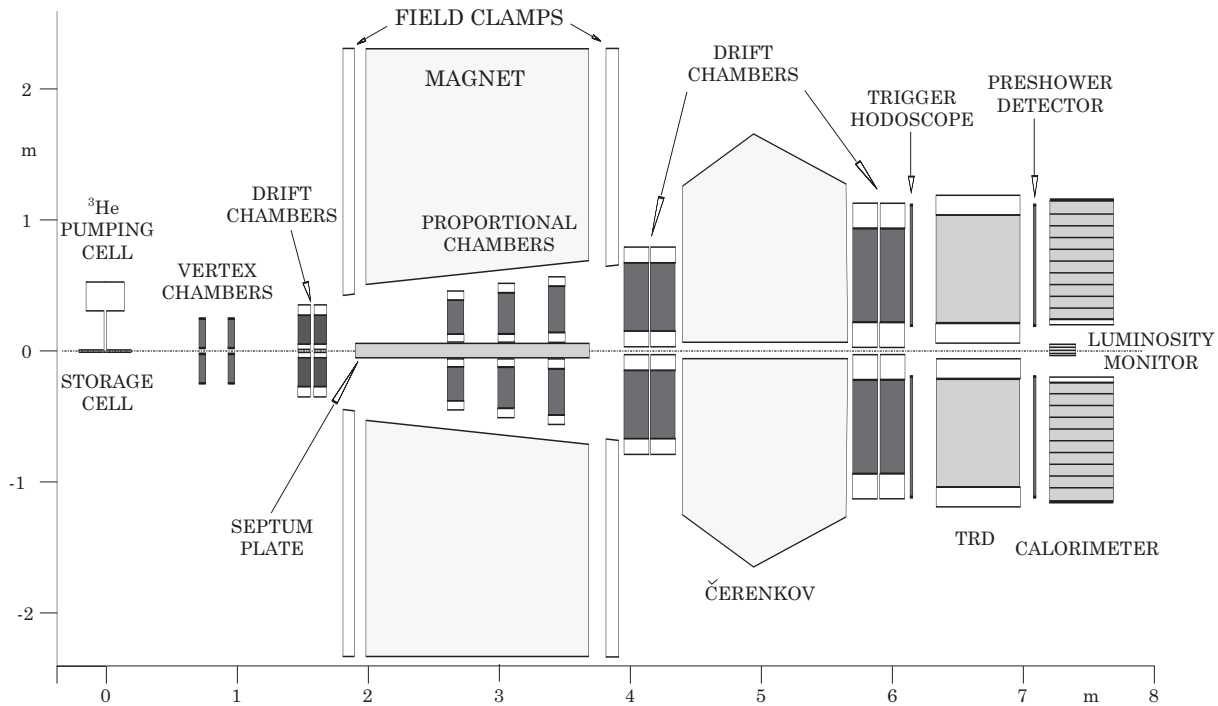


FIG. 1. Schematic diagram of the experimental apparatus (side view).

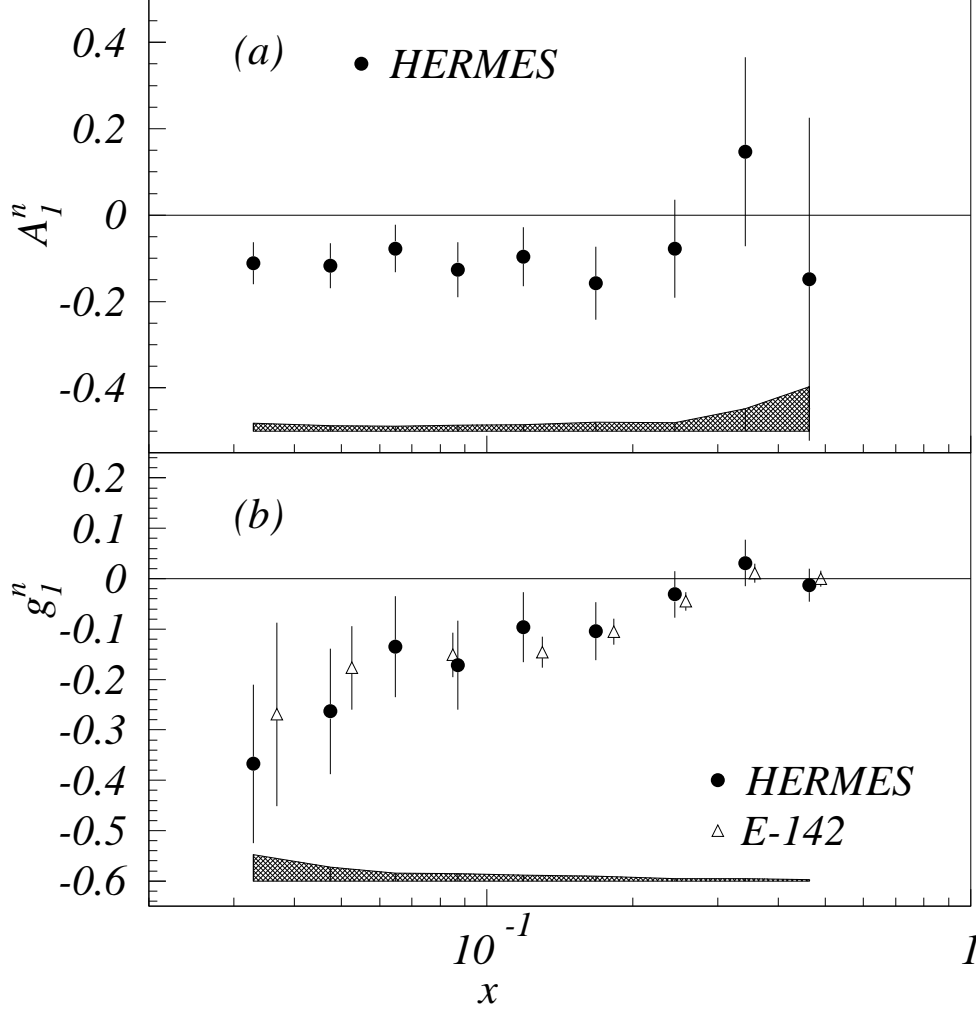


FIG. 2. The spin asymmetry A_1^n (a) and the spin structure function g_1^n (b) of the neutron as a function of x . The values are given for the measured $\langle Q^2 \rangle$. The error bars are statistical uncertainties. The error bands show the systematic uncertainties. The data points from E-142 have been displaced slightly in x for comparison with the present experiment.

TABLE I. Results on $A_1^n(x)$ and $g_1^n(x)$ at the measured Q^2 .

x-range	$\langle x \rangle$	$\langle Q^2 \rangle$ [(GeV/c) ²]	$A_1^n \pm \text{stat.} \pm \text{syst.}$	$g_1^n \pm \text{stat.} \pm \text{syst.}$
0.023-0.040	0.033	1.22	$-0.111 \pm 0.048 \pm 0.018$	$-0.367 \pm 0.157 \pm 0.052$
0.040-0.055	0.047	1.47	$-0.117 \pm 0.052 \pm 0.013$	$-0.263 \pm 0.124 \pm 0.028$
0.055-0.075	0.065	1.73	$-0.077 \pm 0.055 \pm 0.011$	$-0.135 \pm 0.100 \pm 0.016$
0.075-0.10	0.087	1.99	$-0.126 \pm 0.064 \pm 0.014$	$-0.172 \pm 0.088 \pm 0.015$
0.10-0.14	0.119	2.30	$-0.097 \pm 0.068 \pm 0.015$	$-0.096 \pm 0.069 \pm 0.012$
0.14-0.20	0.168	2.65	$-0.158 \pm 0.085 \pm 0.020$	$-0.104 \pm 0.057 \pm 0.010$
0.20-0.30	0.244	3.07	$-0.078 \pm 0.113 \pm 0.019$	$-0.031 \pm 0.046 \pm 0.005$
0.30-0.40	0.342	3.86	$+0.146 \pm 0.219 \pm 0.052$	$+0.031 \pm 0.046 \pm 0.005$
0.40-0.60	0.464	5.25	$-0.149 \pm 0.374 \pm 0.103$	$-0.013 \pm 0.033 \pm 0.003$